DOI:10.1021/ic802228e

Inorganic Chemistry
Article

# Local Coordination of $Fe^{3+}$ in Layered $LiCo_{1-y}Al_yO_2$ Oxides Determined by High-Frequency Electron Paramagnetic Resonance Spectroscopy

**R. Stoyanova,*,† A.-L. Barra,‡ E. Zhecheva,† R. Alcántara,§ G. Ortiz,§ and J.-L. Tirado§**

†*Institute of General and Inorganic Chemistry, Bulgarian Academy of Sciences, 1113 Sofia, Bulgaria,* ‡*Grenoble High Magnetic Field Laboratory, CNRS, 38042 Grenoble Cedex 9, France, and* §*Laboratorio de Química Inorgánica, Facultad de Ciencias, Universidad de Córdoba, 14071 Córdoba, Spain*

Received November 20, 2008

The local coordination of $Fe^{3+}$ spin probes in trigonal $LiAl_yCo_{1-y}O_2$ was studied using high-frequency electron paramagnetic resonance spectroscopy. This technique allows the determination of $Fe^{3+}$ ions in respect to axial and rhombic zero-field splitting parameters (ZFS). After the progressive replacement of Co by Al, the axial *D* parameter of $Fe^{3+}$ increases from +0.0548 to +0.2802 $cm^{-1}$. On the same order, the rhombic *E* parameter decreases. Structural information about the $Fe^{3+}$ site in layered $LiAl_yCo_{1-y}O_2$ oxides was based on modeling of the magnitude of the ZFS parameters by means of the Newman superposition model. It was found that the first metal coordination sphere including $Co^{3+}$ and $Al^{3+}$ ions gave rise to differentiation of the $Fe^{3+}$ dopants in respect to local trigonal and rhombic distortion. The maximum trigonal distortion for the $FeO_6$ octahedron was achieved when $Fe^{3+}$ spin probes were surrounded by Al only, while the Co environment yields a rhombic distortion of the $FeO_6$ octahedron.

## Introduction

Lithium cobaltates, $LiCoO_2$, with a layered structure, belong to the first generation of cathode materials for lithium ion batteries, since they are able to de-intercalate and intercalate lithium reversibly at a potential higher than 4 V.[1,2] The reversible electrochemical extraction of $Li^+$ from $LiO_2$ layers takes place concomitantly with the reversible oxidation of $Co^{3+}$ to $Co^{4+}$ in $CoO_2$ layers.[3,4] One of the ways to manipulate the electrochemical properties of $LiCoO_2$ is by the partial replacement of $Co^{3+}$ with isovalent ions.[4,5] Among several isovalent ions, the most attractive ones are $Al^{3+}$ and $Fe^{3+}$ ions, since they are cheaper and less toxic.[5−12] While $Fe^{3+}$ ions together with $Co^{3+}$ ions participate in the electrochemical reaction, $Al^{3+}$ dopants remain electrochemically inactive. However, a smooth increase in the potential where Li is extracted has been found when Al substitutes for Co.[5−7] The effect of $Al^{3+}$ on the electronic structure of $Co^{3+}$ ions has also been demonstrated by means of $^{27}Al$ magic angle spinning (MAS) NMR spectroscopy.[13] On the basis of the chemical shift of $^{27}Al$, it has been found that every Al nucleus located in the first coordination metal sphere leads to the strengthening of the crystal field of $Co^{3+}$ ions.[13] For Fe-substituted $LiCoO_2$, a novel structural feature has been established by $^{57}Fe$ Mössbauer spectroscopy.[8,9,11,12,14] After partial replacement of the $Co^{3+}$ with $Fe^{3+}$ ($0 < x < 0.2$), $Fe^{3+}$ ions having a smaller isomer shift (0.24−0.19 mm $s^{-1}$) appear. These ions have been assigned to $Fe^{3+}$ ions located in pseudotetrahedral sites in $LiO_2$ layers or in square-pyramidal sites (in $CoO_2$ layers) formed with the participation of an oxygen vacancy.[12,14] The effect of Fe dopants on the structure and electrochemical properties of $LiCoO_2$ is still unclear.

As a very sensitive technique, electron paramagnetic resonance (EPR) spectroscopy is especially suitable for the

*To whom correspondence should be addressed. Phone: +359 02 9793915. Fax: +359 02 8705024. E-mail: radstoy@svr.igic.bas.bg.

(1) Winter, M.; Besenhard, J.; Spahr, M.; Novak, P. *Adv. Mater.* **1998**, *10*, 725–763.
(2) Whittingham, M. S. *Chem. Rev.* **2004**, *104*, 4271–4301.
(3) Ohzuku, T.; Ueda, A.; Nagayama, M.; Iwakoshi, Y.; Komori, H. *Electrochim. Acta* **1993**, *38*, 1159–1167.
(4) Alcantara, R.; Lavela, P.; Tirado, J.-L.; Zhecheva, E.; Stoyanova, R. *J. Solid State Electrochem.* **1999**, *3*, 121–134.
(5) Ceder, G.; Chiang, Y.-M.; Sadoway, D. R.; Aydinol, M. K.; Jang, Y.-I.; Huang, B. *Nature (London)* **1998**, 392.
(6) Alcántara, R.; Lavela, P.; Relaño, P. L.; Tirado, J. L.; Zhecheva, E.; Stoyanova, R. *Inorg. Chem.* **1998**, *37*, 264–269.
(7) Yoon, W.-S.; Lee, K.-K.; Kim, K.-B. *J. Electrochem. Soc.* **2000**, *147*, 2023–2028.
(8) Alcántara, R.; Jumas, J. C.; Lavela, P.; Olivier-Fourcade, J.; Pérez-Vicente, C.; Tirado, J. L. *J. Power Sources* **1999**, *81−82*, 547–553.
(9) Tabuchi, M.; Ado, K.; Kobayashi, H.; Sakaebe, H.; Kageyama, H.; Masquelier, C.; Yonemura, M.; Hirano, A.; Kanno, R. *J. Mater. Chem.* **1999**, *9*, 199.
(10) Holzapfel, M.; Schreiner, R.; Ott, A. *Electrochim. Acta* **2001**, *46*, 1063–1070.
(11) McLaren, V. L.; West, A. R.; Tabuchi, M.; Nakashima, A.; Takahara, H.; Kobayashi, H.; Sakaebe, H.; Kageyama, H.; Hirano, A.; Takeda, Y. *J. Electrochem. Soc.* **2004**, *151*, A672–A681.
(12) Aldon, L.; Olivier-Fourcade, J.; Jumas, J.-C.; Holzapfel, M.; Darie, C.; Strobel, P. *J. Power Sources* **2005**, *146*, 259–263.
(13) Gaudin, E.; Taulelle, F.; Stoyanova, R.; Zhecheva, E.; Alcantara, R.; Lavela, P.; Tirado, J. L. *J. Phys. Chem. B* **2001**, *105*, 8081–8087.
(14) Ménétrier, M.; Shao-Horn, Y.; Wattiaux, A.; Fournés, L.; Delmas, C. *Chem. Mater.* **2005**, *17*, 4653–4659.


Published on Web 4/13/2009

determination of the immediate environment of transition metal ions. For example, the effect of mixed Co/Al neighbors on both the symmetry and the strength of the crystal field of transition metal ions has been demonstrated by analyzing the EPR spectra of low-spin $Ni^{3+}$ ions used as spin probes in layered $LiAl_yCo_{1-y}O_2$ and $LiGa_yCo_{1-y}O_2$.[15,16] A local tetragonal distortion of $Ni^{3+}$ ions is observed when they are located in a mixed $Co_{6-y}Al_y$ environment.[15] The strength of the crystal field for $Ni^{3+}$ increases gradually, and the extent of the tetragonal distortion shows a tendency to increase along the progressive replacement of Co by Al.[15]

Here, we extend our study concerning the effect of metal neighbors on the symmetry and the strength of the crystal field of transition metal ions in layered $LiAl_yCo_{1-y}O_2$ oxides by using $Fe^{3+}$ as spin probes. An important piece of information coming from the analysis of EPR spectra of $Fe^{3+}$ ions is the splitting of the six magnetic sublevels of the ground state $S = 5/2$ level into zero-magnetic field (zero-field splitting, ZFS).[17−19] This splitting is parametrized by a term in the phenomenological spin-Hamiltonian that is biquadratic in the electron spin:

$$H = \beta S g \mathbf{B} + D[S_z^2 - S(S+1)/3 + (E/D)(S_x^2 - S_y^2) \quad (1)$$

where $\beta$ is the Bohr magneton and **B** is the applied magnetic field. The parameters that are highly sensitive toward the local environment are the axial and rhombic ZFS parameters ($D$ and $E$, respectively). Going from axial to rhombic symmetry, the $E$-to-$D$ ratio varies from 0 to 1/3. Depending on the magnitude of the $D$ parameter in regard to the microwave quantum, the EPR response of the system can be divided into two different cases:[18] (i) low-field approximation where $D$ values are smaller than $h\nu$ and (ii) high-field approximation with $D \gg h\nu$. The first case is usually met with the conventional X-band EPR experiments ($h\nu \approx 0.3$ cm$^{-1}$), as a result of which the determination of ZFS parameters is not unambiguous. For accurate determination of the ZFS parameters, the use of microwave frequencies exceeding the fine structure interactions is needed.[19]

Due to the lack of orbital angular momentum for the $Fe^{3+}$ ground state ($^6S_{5/2}$), the **g** matrix has usually very small anisotropy, while the origin of the ZFS parameters is complex. Several mechanisms comprising the direct dipole−dipole interaction of unpaired electrons and the spin−orbit coupling of excited states into the ground state contribute to the ZFS.[20,21] Among them, it is accepted that spin−orbit coupling is dominant for $Fe^{3+}$ complexes.[20,21] For structural modeling of the local environment, it has been shown that the ZFS parameters can be calculated in the framework of the semiempirical Newman superposition model (NSM).[22,23] According to this model, ZFS parameters are regarded by a superposition of individual contributions of separate neighboring ligands. The assumption is that the contribution of ligands is restricted toward the nearest neighbors, and the interaction between the ligands is ignored. The NSM expression for the zero-field splitting parameters is as follows:

$$b_2^q = 3\bar{b}_2(R_o)\sum_i \left(\frac{R_o}{R_i}\right)^{t_k} K_2^q(\Theta_i, \phi_i) \quad (2)$$

where $b_2^q$ represents the fine-structure parameters, which are related to the experimentally available axial and rhombic ZFS: $D = b_2^o$ and $E = 1/3b_2^2$.[23,24] Here, $R_i$ is the distance between the $i$th ligand and the paramagnetic ion, $\Theta_i$ and $\varphi_i$ are the polar and axial angles, and $K_2^q$ denotes the coordination factor that, for a trigonal symmetry, is expressed by $K_2^o = {}^1/_2(3\cos^2\Theta - 1)$ and $K_2^2 = {}^3/_2\sin^2\Theta\cos 2\varphi$.[23−25] The power-law exponent $t_k$ and single ligand contribution $b_2(R_0)$ are specific for a particular ion−ligand system. As a semiempirical model, the superposition model has shown to be quite successful in explaining the crystal field splitting.

The aim of this study is to determine the local coordination of $Fe^{3+}$ spin probes in layered $LiAl_yCo_{1-y}O_2$ oxides by using high-frequency EPR (HF-EPR). Solid solutions between $LiCoO_2$ and $LiAlO_2$ were prepared by the citrate precursor method. On the basis of $^{27}$Al NMR, it has been shown that this method is suitable for the preparation of $LiAl_yCo_{1-y}O_2$ oxides in which Co and Al are statistically distributed within the layers.[13] Structural information about the $Fe^{3+}$ site in layered $LiCo_{1-y}Al_yO_2$ oxides was based on modeling the magnitude of the ZFS parameter in terms of the Newman superposition model. For the determination of the ZFS parameter, HF-EPR spectroscopy was undertaken.

## Experimental Section

Samples of $LiAl_yCo_{1-y}O_2$ with $0 \le y \le 0.8$ were prepared by the citrate precursor method, as described elsewhere.[13] This method consists of the thermal decomposition of freeze-dried Li−Co−Al−citrate complexes and permits the obtainment of pure $LiAl_yCo_{1-y}O_2$ solid solutions. Lithium−cobalt−aluminum−citric acid compositions were obtained by dissolving $Li_2CO_3$, $CoCO_3$, and $Al(NO_3)_3\cdot 9H_2O$ in aqueous solutions of citric acid (0.1 M) at 80 °C. The ratio between the components was as follows: Li/(Co + Al)/Cit = 1:1:1 and Al/(Co + Al) = 0, 0.1, 0.5, and 0.8. In this solution, iron nitrate of a low concentration level was added (Fe/(Fe + Co + Al) = 0.005). After complexation, the solution obtained was cooled down to room temperature, then frozen instantly with liquid nitrogen and dried in a vacuum (20−30 mbars) at −20 °C with an Alpha-Crist Freeze-Dryer. After drying, the solid residues were decomposed at 450 °C with a heating rate of 1°/min and were further heated at 800 °C for 24 h. For the sake of comparison, a commercial LiCoO2 (Aldrich, Lot #20804PR) containing ≤ 0.002% Fe was used.

The metal content of the samples was determined by atomic absorption analysis. The mean oxidation state of cobalt was determined by iodometric titration.

X-ray structural analysis was made using a Bruker Advance 8 diffractometer with Cu Kα radiation. Step-scan recordings for structure refinement by the Rietveld method were carried out using 0.03° 2$\theta$ steps of 10 s duration. The computer program FULLPROF was used in the calculations.[26] In agreement with previous structural characterization,[13] the

(15) Stoyanova, R.; Zhecheva, E.; Alcántara, R.; Tirado, J. L. *J. Phys. Chem. B* **2004**, *108*, 4053–4057.
(16) Zhecheva, E.; Stoyanova, R.; Alcántara, R.; Tirado, J. L. *J. Phys. Chem. B* **2003**, *107*, 4290–4295.
(17) Hagen, W. R. *Coord. Chem. Rev.* **1999**, *192*, 209–229.
(18) Anderson, K. K.; Schmidt, P. P.; Ketterle, B.; Strand, K.; Palmer, A.; Lee, S.-K.; Solomon, E. I.; Gräslund, A.; Barra, A.-L. *J. Biol. Inorg. Chem.* **2003**, *8*, 235–247.
(19) Krzystek, J.; Ozarowski, A.; Telser, J. *Coord. Chem. Rev.* **2006**, *250*, 2308–2324.
(20) Wan-Lu, Y.; Min-Guang, Z. *Phys. Rev. B* **1988**, *37*, 9254–9267.
(21) Zein, S.; Duboc, C.; Lubitz, W.; Neese, F. *Inorg. Chem.* **2008**, *47*, 134–142.
(22) Newman, D. J. *Adv. Phys.* **1971**, *20*, 197.
(23) Newman, D. J.; Ng, B. *Rep. Prog. Phys.* **1989**, *52*, 699.
(24) Rudowich, C.; Madhu, S. *J. Phys.: Condens. Matter* **1999**, *11*, 273.
(25) Siegel, E.; Müller, K. A. *Phys. Rev. B* **1979**, *20*, 3587–3596.
(26) Rodriguez-Carvajal, J. In *Satellite Meeting on Powder Diffraction of the XV Congress of the IUCr*; International Union of Crystallography: Chester, England, 1990; p 127

structural model used comprised Li in 3*b* sites (0 0 0.5), $Co_{1-y}Al_y$ in 3*a* sites (0 0 0), and oxygen in 6*c* sites (0 0 z) for the $R\bar{3}m$ space group. The Li/(Co + Al) and Al/(Co + Al) ratios were imposed by the chemical composition of the oxides. The Fe dopants (0.5%) are not included in the refinement procedure due to the close scattering factors of Co and Fe. The refined structural parameters are as follows: $a = 2.8153$, $c = 14.0495$, and $z = 0.2592$ for $LiCoO_2$; $a = 2.8128$, $c = 14.0908$, and $z = 0.2595$ for $LiAl_{0.1}Co_{0.9}O_2$; $a = 2.8069$, $c = 14.1736$, and $z = 0.2599$ for $LiAl_{0.5}Co_{0.5}O_2$; $a = 2.8028$, $c = 14.2169$, and $z = 0.2620$ for $LiAl_{0.8}Co_{0.2}O_2$. It is noticeable that the crystal structure parameters of Fe-doped and undoped $LiAl_yCo_{1-y}O_2$ oxides remain the same. For the sake of comparison, the structural parameters for layered modification of $LiAlO_2$ (prepared at atmospheric pressure) are $a = 2.7993$ and $c = 14.18$.[27]

EPR measurements at 9.23 GHz (X-band) were carried out in a ERS 220/Q spectrometer within the temperature range 85−410 K. The *g* factors were established with respect to a $Mn^{2+}$/ZnS standard. The high-frequency EPR spectra were recorded on a single-pass transmission EPR spectrometer built at the High-Magnetic Field Laboratory, Grenoble, France. The frequencies were changed from 95 to 345 GHz using Gunn diodes and their multipliers. The detection of absorption was performed with a bolometer. The recording temperatures were varied from 5 to 300 K using a variable-temperature insert (Oxford Instruments). The simulation software SIM written by Weihe was used to extract numerical values of spin Hamiltonian parameters from experimental EPR spectra. [28,29] The program is based on a full-matrix diagonalization procedure and allows generation of the powder pattern EPR spectra of spin systems with any values of zero-filed splitting parameters relative to the operating frequencies. This program also takes into account the Boltzman population factor in calculating the EPR intensities. The Lorentzian line shape and a line width varying between 5.5 and 7.5 mT were used in the fitting procedure.

## Results

**EPR Spectroscopy of $Fe^{3+}$ Spin Probes in Layered $LiCoO_2$.** Figure 1 shows the X-band EPR spectra of $Fe^{3+}$ dopants in layered $LiCoO_2$. As one can see, the EPR signals simultaneously broaden with an increase in the Fe content, but the EPR patterns remain unchanged. This indicates that the EPR signal comes from $Fe^{3+}$.

The EPR spectrum consists of several resonance lines spanned over a wide field range. The two sets of lines with effective *g* values of 4.9/4.0 and 2.0/1.9 are well distinguished, while the other sets of lines are with lower intensities and higher line widths. These powder EPR patterns imply that a low-field approximation model is fulfilled, that is, the *D* parameter of $Fe^{3+}$ has a value comparable with the energy of the microwave frequency ($h\nu \approx 0.3$ cm$^{-1}$). The signal splitting at about 160 mT and 330 mT points to an increased $|E/D|$ ratio, which is expected to vary from 1/5 to 1/4. In addition, a single Lorentzian line with $g = 2.14$ is superimposed onto the EPR signal of $Fe^{3+}$. This signal has been assigned to a low-spin $Ni^{3+}$ impurity. Due to the high sensitivity of the EPR spectroscopy in the X region, even small amounts of paramagnetic $Ni^{3+}$ ions replacing $Co^{3+}$ in the diamagnetic

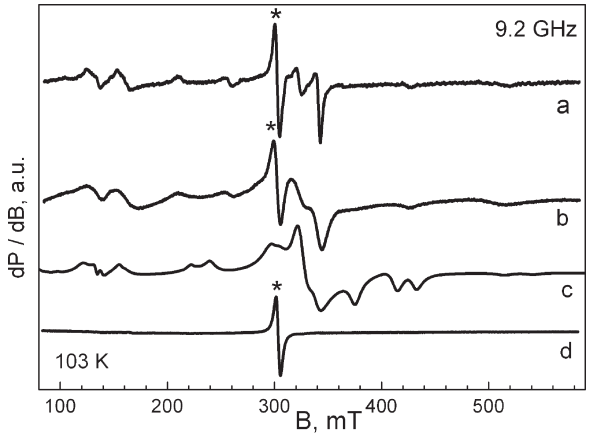


**Figure 1.** Experimental X-band EPR spectrum of $Fe^{3+}$ in layered $LiCoO_2$ containing 0.002% Fe (a), $LiFe_{0.005}Co_{0.995}O_2$ (b), simulated EPR spectrum of $Fe^{3+}$ with $D = 0.0495$ cm$^{-1}$ and $|E/D| = 0.236$ (c), and experimental EPR spectrum of $Ni^{3+}$ ions in $LiNi_{0.005}Co_{0.995}O_2$ (d). The asterisk denotes the impurity $Ni^{3+}$ ions.

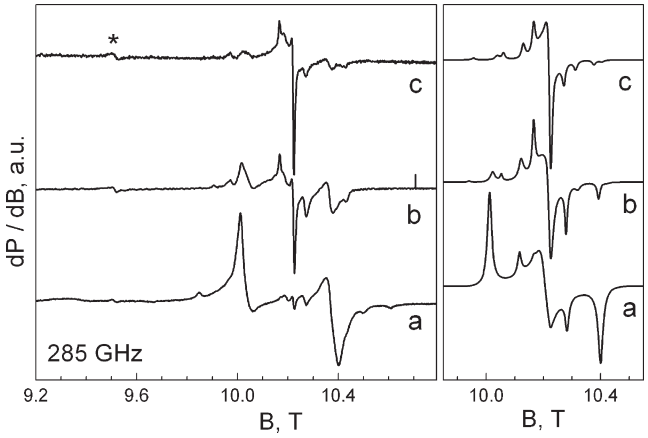


**Figure 2.** Experimental (left) and simulated (right) EPR spectra at 285 GHz of $Fe^{3+}$ in layered $LiFe_{0.005}Co_{0.995}O_2$. The operating temperature is 5 K (a), 30 K (b), and 100 K (c). The asterisk denotes the signal due to the impurity $Ni^{3+}$ ions.

$LiAl_yCo_{1-y}O_2$ can be detected by EPR (less than 0.05%, which is the common impurity content for cobalt salts without special purification). [30,6]

To determine *D* and *E* parameters, the use of high frequencies is needed. Figure 2 presents the HF-EPR spectrum of $Fe^{3+}$ spin probes in $LiCoO_2$. As one can expect, the high-field approximation is fulfilled when the EPR spectrum is registered at 285 GHz (Figure 2). At 100 K, the HF-EPR spectrum consists of a central signal with tetragonal symmetry. The values of the **g** tensor are as follows: $g_\perp = 1.9921$ and $g_\parallel = 2.0027$. The small anisotropy in the **g** tensor of $Fe^{3+}$ has been reported for iron-doped $LiNbO_3$ where $g_\parallel > g_\perp$. [31] In addition, weaker signals that are shifted downfield and upfield, as compared to the central tetragonal signal, become visible. On cooling, the intensity of the central tetragonal signal decreases at the expense of the outer signals. At 5 K, the two intensive outermost signals at 10.0 and 10.4 T dominate the EPR spectrum. It is noticeable that the

(27) Poeppelmeier, K. R.; Chiang, C. K.; Kipp, D. O. *Inorg. Chem.* **1988**, *27*, 4523–4524.
(28) Glerup, J.; Weihe, H. *Acta Chem. Scand.* **1991**, *45*, 444.
(29) Weihe, H. *SIM*; Institute of Chemistry, University of Copenhagen: Copenhagen, Denmark.
(30) Stoyanova, R.; Zhecheva, E.; Alcantara, R.; Lavela, P.; Tirado, J.-L. *Solid State Commun.* **1997**, *102*, 457–462.
(31) Keeble, D. J.; Loyo-Menoy, M.; Furukawa, Y.; Kitamura, K. *Phys. Rev. B* **2005**, *71*, 224111.

outermost signals are broadened as compared to the central tetragonal signal.

The structured EPR pattern of $Fe^{3+}$ ions can be understood taking into account the FS interactions for the high-field approximation.[18,32] According to these conditions, the central tetragonal signal corresponds to the $|-1/2>$ to $|+1/2>$ transition, while outer lines come from non-central allowed transitions ($|\pm5/2>$ to $|\pm3/2>$ and $|\pm3/2>$ to $|\pm1/2>$, respectively). The line positions depend on both the magnitude of $D$ and the $E$-to-$D$ ratio, while the line intensities reflect the population of $(2S + 1)$ states. For the axially symmetric system ($E/D = 0$), there are three sets of lines shifted from the central line at $\pm4D$, $\pm2D$, and $\pm D$, while for the rhombic system ($E/D = 1/3$), two set of lines at $\pm4D$ and $\pm2D$ appear. [32] In the intermediate case ($0 < E/D < 1/3$), the lines are split, and the EPR spectrum becomes more complex. [18,32] By increasing the microwave frequency and by lowering the operating temperature, only the lowest energy level of the $S$ multiplet is thermally populated, which simplifies the complex EPR spectrum. This is known as the polarization effect of HF-EPR spectroscopy: at 285 GHz, the polarization effect appears below 15 K.[18]

The frequency and temperature dependence of the position and intensity of the structured EPR spectrum allows a rough estimation of the magnitudes of the $D$ and $E$ parameters. In addition, the variation in the EPR patterns indicates that only one type of $Fe^{3+}$ ion gives rise to the EPR spectrum of $LiCoO_2$. For $Fe^{3+}$ in pure $LiCoO_2$, the observed distance between the central line and the outermost line indicates that the $D$ value has to be about 55 mT, while the line splitting is consistent with an $E$-to-$D$ ratio slightly lower than 1/3. The suggested value of the $E$-to-$D$ ratio is in agreement with that expected from the X-band EPR spectrum: $1/5 < |E/D| < 1/4$. Using these values as initial parameters, the powder EPR spectrum is generated by a simulation program written by Weihe.[28,29] By comparing the generated EPR spectrum with the experimental one, the refined $D$ and $E$ parameters are determined and are shown in Table 1. The broadening of the outermost signals as compared to the central tetragonal signal is related to a $D$-strain contribution to the EPR line width. The introduction of the $D$-strain broadening leads to the improvement of the fitting procedure: $\delta D = 0.0007$ cm$^{-1}$. As one can see from Table 1, the $D$ parameter increases with a lowering of the operating temperature, while the $E$-to-$D$ ratio slightly decreases. Since the $E$-to-$D$ ratio is higher than 0.2, the sign of $D$ has no physical meaning. However, for the simulation of the EPR spectra, the positive $D$ value was used. To check the correctness of experimentally obtained $D$ and $E$ parameters, Figure 1 displays the simulated EPR spectrum at a lower frequency (9.23 GHz, X-band experiments). As one can see, there is satisfactory agreement between the experimental and simulated EPR spectra.

**EPR Spectroscopy of $Fe^{3+}$ Spin Probes in $LiAl_yCo_{1-y}O_2$ Solid Solutions.** When Al substitutes for Co in $LiAl_yCo_{1-y}O_2$, the EPR spectrum of $Fe^{3+}$ spin probes undergoes strong changes (Figure 3). By increasing the Al content, the central signal is split into several components.

**Table 1.** $g$-Tensor and ZFS Parameters for $Fe^{3+}$-Doped $LiAl_yCo_{1-y}O_2$ Host

| matrix | $g_1$ | $g_2$ | $g_3$ | $D$, cm$^{-1}$ | $E/D$ |
|---|---|---|---|---|---|
| $LiAl_{0.8}Co_{0.2}O_2$ | 1.9976 | 1.9984 | 2.0030 | 0.2802 | *0.078* |
| | 1.9973 | 1.9980 | 2.0028 | 0.2362 | *0.166* |
| | 1.9973 | 1.9978 | 2.0026 | 0.2015 | *0.225* |
| | 1.9968 | 1.9968 | 2.0026 | 0.1768 | *0.327* |
| $LiAl_{0.5}Co_{0.5}O_2$ | 1.9948 | 1.9956 | 2.0024 | 0.2361 | *0.201* |
| | 1.9951 | 1.9958 | 2.0022 | 0.1941 | *0.199* |
| | 1.9948 | 1.9960 | 2.0028 | 0.1684 | *0.074* |
| | 1.9951 | 1.9958 | 2.0017 | 0.0871 | *0.026* |
| $LiAl_{0.1}Co_{0.9}O_2$ | 1.9926 | 1.9933 | 2.0030 | 0.0912 | *0.329* |
| $LiCoO_2$ | 1.9911 | 1.9922 | 2.0030 | 0.0545 | *0.262* |
| $LiCoO_2$ ($T$ = 30K) | 1.9911 | 1.992 | 2.0030 | 0.0528 | *0.250* |
| $LiCoO_2$ ($T$ = 100K) | 1.9911 | 1.9922 | 2.0030 | 0.0492 | *0.242* |
| $Fe^{3+}$ in the Co site of $LiCoO_2$[a] | | | | 0.305 | |
| $Fe^{3+}$ in the Li site of $LiCoO_2$[a] | | | | −0.225 | |

[a] Calculated using the superposition model.

In the same sequence, the number of the upperfield lines increases and becomes higher as compared to the number of downfield lines. As in the case of $Fe^{3+}$ in pure $LiCoO_2$, the intensity of the central signal increases with increasing operating temperature, while the intensities of the outer lines decrease. In addition, the outermost signals remain broadened as compared to the central lines. Close inspection of Figure 3 shows that the EPR spectra of $Fe^{3+}$ in intermediate compositions (containing 10 and 50% Al) can be presented as a convolution of the EPR spectra of $Fe^{3+}$ in two end compositions: $LiCoO_2$ and $LiAl_{0.8}Co_{0.2}O_2$.

For $LiAl_{0.8}Co_{0.2}O_2$, the two outermost signals (at 9.44 and 11.34 T) are significantly shifted as compared to those observed for $Fe^{3+}$ in pure $LiCoO_2$ (at 10.00 and 10.40 T). The increased distance between the downfield line and the central line indicates an increased magnitude of the $D$ parameter, reaching a maximum of 280 mT. The higher number of upperfield lines can be simulated if we suppose that the $D$ parameter and the $E$-to-$D$ ratio take several values. The procedure to extract numerical values of $D$ and $E$ parameters was the same as in the case of $Fe^{3+}$ in pure $LiCoO_2$. Figure 4 shows the contribution of each $Fe^{3+}$ ion (having different ZFS parameters) to the EPR patterns of Fe-doped $LiAl_{0.8}Co_{0.2}O_2$. The refined $D$ and $E$ parameters of $Fe^{3+}$ in $LiAl_{0.8}Co_{0.2}O_2$ are also given in Table 1. It appears that the $D$ parameter possesses discrete values which are spread from 0.17 to 0.28 cm$^{-1}$. In all cases, the $D$ values for $Fe^{3+}$ in $LiAl_{0.8}Co_{0.2}O_2$ are greater compared to that of $Fe^{3+}$ in pure $LiCoO_2$ ($D = 0.0548$ cm$^{-1}$). The $E$-to-$D$ ratio varies from 0.05 to 0.33 for $Fe^{3+}$ in $LiAl_{0.8}Co_{0.2}O_2$ oxides. The sign of $D$ is determined in the case when the $E$-to-$D$ ratio is lower than 0.2. From the temperature variation of the EPR transitions, it appears that the $D$ parameter is positive.

For intermediate compositions containing 10 and 50% Al, the outer signals become broader. As in the case of $Fe^{3+}$ in $LiAl_{0.8}Co_{0.2}O_2$, the fitting of experimental EPR spectra is achieved by invoking $Fe^{3+}$ species having different $D$ and $E$ parameters. The refined values are shown in Table 1. By increasing the Al content, the magnitude of $D$ increases together with a decrease in the $E$-to-$D$ ratio.

To check the correctness of the experimentally obtained $D$ and $E$ parameters, EPR experiments at lower

(32) Wood, R. M.; Stucker, D. M.; Jones, L. M.; Bryan Lunch, W.; Misra, S. K.; Freed, J. H. *Inorg. Chem.* **1999**, *38*, 5384–5388.

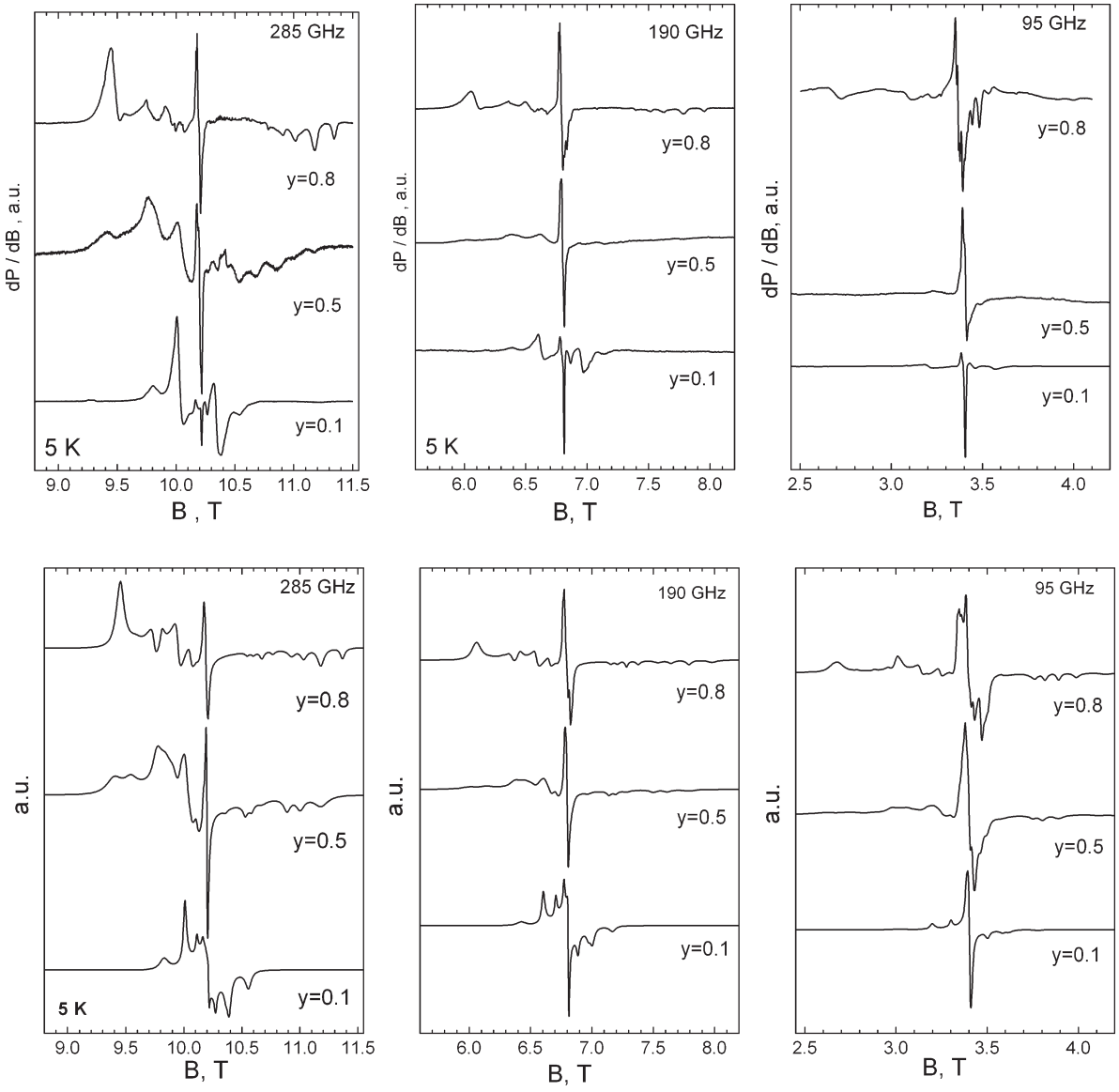


**Figure 3.** Experimental (top) and simulated (bottom) EPR spectra at 285, 190, and 95 GHz of $Fe^{3+}$ in layered $LiFe_{0.005}(Al_yCo_{1-y})_{0.995}O_2$ with $y = 0.1, 0.5,$ and 0.8. The operating temperature is 5 K.

frequencies were undertaken. Figure 3 gives the $Fe^{3+}$ EPR spectra registered at 95 and 190 GHz. Using the *D* and *E* values determined at 285 GHz, the same figure gives the simulated EPR spectra at these frequencies. As one can see, there is a satisfactory agreement between the experimental and simulated EPR spectra. In the X-band experiments, the EPR spectra display an intensive signal with an effective *g* value at about 6 (Figure 5). This means that the signal coming from $Fe^{3+}$ with a lower *E*-to-*D* ratio dominates in the EPR spectra of $LiAl_{0.8}Co_{0.2}O_2$ oxides.

## Discussions

The experimentally determined fine-structure parameters (*D* and *E)* for the $Fe^{3+}$ ion allow us to analyze the local coordination of $Fe^{3+}$ in $LiAl_yCo_{1-y}O_2$ oxides. The crystal structure of $LiAl_yCo_{1-y}O_2$ (space group $R\bar{3}m$, α-$NaFeO_2$-type) is composed of a consecutive arrangement of $Li^+$ and $Al_yCo^{3+}_{1-y}$ ions in the close-packed oxygen arrays, leading to the formation of discrete lithium and cobalt−aluminum layers.[27,33,34] The metal layers are built of edge-sharing $MO_6$ octahedra where the host site symmetry is the trigonally distorted octahedron (Figure 6). If $Fe^{3+}$ occupies the trigonal host site, the *D* parameter can be expressed within the framework of the semiempirical superposition model as follows:

$$b_2^0 = 3b_2^-(R_o)\left(\frac{R_o}{R}\right)^{t_2}(3\cos^2\Theta - 1) \qquad (3)$$

where *R* is the Fe−O bond length and the trigonal distortion angle Θ stands for the angle between the Fe−O bond and the 3-fold axis (for the undistorted octahedron, the Θ value is 54.74 °). These structural parameters are shematically presented in Figure 6. For the trigonal host site, the *E* parameter

(33) Orman, H. J.; Wiseman, P. J. *Acta Crystallogr., Sect. C* **1984**, *40* 12–14.
(34) Marezio, M.; Remeika, J. P. *J. Chem. Phys.* **1966**, *44*, 3143.

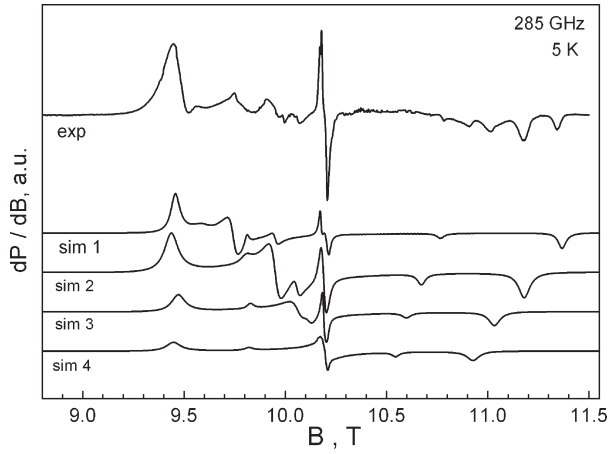


**Figure 4.** Experimental EPR spectrum of $Fe^{3+}$ in layered $LiFe_{0.005}(Al_{0.8}Co_{0.2})_{0.995}O_2$ and simulated EPR spectra for $Fe^{3+}$ with $D = 0.2802\ cm^{-1}$ and $E/D = 0.078$ (sim 1), $D = 0.2362\ cm^{-1}$ and $E/D = 0.166$ (sim 2), $D = 0.2015\ cm^{-1}$ and $E/D = 0.225$ (sim 3), and $D = 0.1768\ cm^{-1}$ and $E/D = 0.327$ (sim 4).

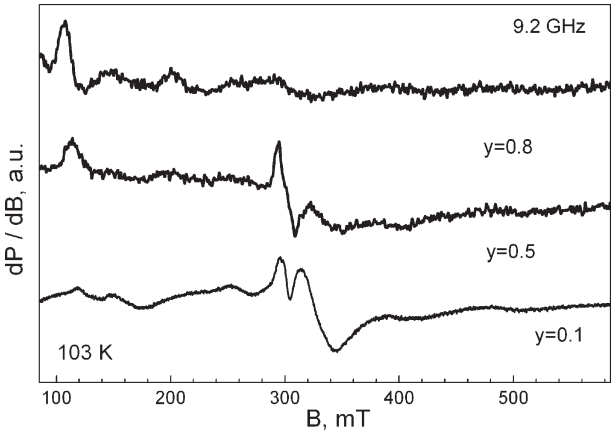


**Figure 5.** Experimental X-band EPR spectrum of $Fe^{3+}$ in layered $LiFe_{0.005}(Al_yCo_{1-y})_{0.995}O_2$ oxides with $y = 0.1$, 0.5, and 0.8. The operating temperature is 103 K.

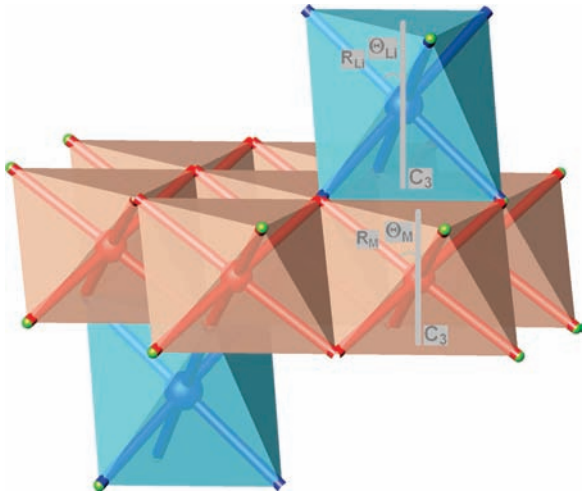


**Figure 6.** Schematic representations of lithium and cobalt sites in $LiCoO_2$ (blue and red octahedra, respectively). The metal−oxygen bond length ($R_M$ and $R_M$), trigonal distortion angle ($\Theta_{Li}$ and $\Theta_M$), and $C_3$ axis are also shown.

has to be zero. From this equation, it is clear that the adaptation of adequate intrinsic parameters $t_2$ and $b(R_o)$ is of significance. Taking into account the available literature data on $Fe^{3+}$ in different matrices (such as $PbTiO_3$, $SrTiO_3$, $BaTiO_3$, $PbZrO_3$, $LiTaO_3$, and $LiNbO_3$[25,31,35−39]), the intrinsic parameters of $Fe^{3+}$ in MgO are successfully adopted for the determination of the local $Fe^{3+}$ environment. These parameters are $t_2 = 8$, $\overline{b}(R_o) = -0.412\ cm^{-1}$, and $R_o = 2.101$ Å.[25,35] In our analysis, we also used these parameters. For the determination of the host $Al_yCo_{1-y}$−O bond length and the host trigonal angle Θ, the positions of oxygen atoms surrounding Li and $Al_yCo_{1-y}$ ions in the layers were taken from the Rietveld refinement of powder XRD patterns of $LiAl_yCo_{1-y}O_2$.

Table 1 gives the calculated values of the $D$ parameter for $Fe^{3+}$ supposing that $Fe^{3+}$ occupies a Li or $Co_{1-y}Al_y$ site. The important finding is that the sign of $D$ is changed from negative to positive when $Fe^{3+}$ ions are moved from the Li to the $Co_{1-y}Al_y$ site, that is, from a trigonally elongated octahedron to a trigonally compressed octahedron. This feature is supported by experimental data on $Fe^{3+}$ dopants in several matrices. For example, $Fe^{3+}$ dopants in a $CdCl_2$ matrix adopting a trigonally compressed local environment ($R = 2.404$ Å and $\theta = 59.02$) possess a positive $D$ parameter ($+0.1697\ cm^{-1}$),[40] while $Fe^{3+}$ centers located in a trigonally elongated octahedron ($2.039 \le R \le 2.075$ Å and $53.566 \le \Theta \le 53.867°$) in germanate garnets $Ca_3M_2Ge_3O_{12}$ (M = Al, Ga, Sc, In, Lu) exhibits a negative $D$ parameter (varying from $-0.0405$ to $-0.0367\ cm^{-1}$).[41] Analysis of the HF-EPR spectra of $Fe^{3+}$ in layered $LiAl_yCo_{1-y}O_2$ oxides shows that the $D$ parameter has a positive sign. This means that $Fe^{3+}$ occupies a trigonally compressed site, which is available in the $Al_yCo_{1-y}O_2$ layers.

From eq 3, it is clear that the magnitude of the $D$ parameter will increase with the increasing extent of trigonal distortion of the $FeO_6$ octahedron and with the lowering of the Fe−O bond length. For Al-containing oxides, the host $Co_{0.2}Al_{0.8}O_6$ octahedron is more distorted and the mean $Co_{0.2}Al_{0.8}$−O bond length is shorter as compared to the Co-host site: $R = 1.91$ Å and $\Theta = 57.93$ for $Co_{0.2}Al_{0.8}O_6$ and $R = 1.93$ Å and $\Theta = 57.35$ for $CoO_6$. As a result, the $D$ value of $Fe^{3+}$ in $LiAl_yCo_{1-y}O_2$ has to be higher than that of $Fe^{3+}$ in Co analogues. This suggestion is consistent with the observation that the $D$ magnitude increases with the Al content. However, a comparison shows that the experimentally obtained $D$ values are lower in regard to that calculated if $Fe^{3+}$ substitutes isomorphically for $Co^{3+}$ or $Al^{3+}/Co^{3+}$ ions in transition metal layers of $LiCoO_2$ or $LiAl_{0.8}Co_{0.2}O_2$, respectively. This discrepancy indicates a local structural distortion around $Fe^{3+}$ ions located in the transition metal layers. From the lower $D$ values, it appears that the local structural

(35) Siegel, E.; Müller, K. A. *Phys. Rev. B* **1979**, *19*, 109–120.
(36) Meštrić, H.; Eichel, R.-A.; Kloss, T.; Dinse, K.-P.; Laubach, So.; Laubach, St.; Schmidt, P. C.; Schönau, K. A.; Knapp, M.; Ehrenberg, H. *Phys. Rev B* **2005**, *71*, 134109.
(37) Meštrić, H.; Eichel, R.-A.; Dinse, K.-P.; Ozarowski, A.; van Tol, J.; Brunel, L. C.; Kungl, H.; Hoffmann, M. J.; Schönau, K. A.; Knapp, M.; Fuess, H. *Phys. Rev. B* **2006**, *73*, 184105.
(38) Yeom, T. H. *J. Phys.: Condens. Matter* **2001**, *13*, 10471–10476.
(39) Zhao, M. G.; Chiu, M. *Phys. Rev. B* **1994**, *49*, 12556–12558.
(40) Cheng, L.; Yu, K. X.; Wei, Z. K. *Solid State Commun.* **2008**, *145* 565–570.
(41) Zhang, C.-X.; Kuang, X.-Y.; Li, G.-D.; Wang, H. *Chem. Phys. Lett.* **2007**, *441*, 143–147.

distortion comprises the increased Fe−O bond length and reduced extent of the trigonal distortion as compared to the host site structure. The ionic size mismatch of $Co^{3+}$, $Al^{3+}$, and $Fe^{3+}$ ions can be regarded as a driving force for local structural distortion: while $Co^{3+}$ and $Al^{3+}$ have close ionic sizes (0.525 and 0.53 Å), the ionic radius of $Fe^{3+}$ is significantly higher (0.645 Å). Supporting this suggestion, there is an increase in the mean bond lengths of Co−O, Al−O, and Fe−O in layered $LiCoO_2$, $LiAlO_2$, and $LiFeO_2$ analogues: 1.930, 1.926, and 2.035 Å, respectively.[13,42] In the same sequence, the extent of the trigonal distortion decreases: 57.35, 57.05, and 56.85, respectively. Since the Co−O and Al−O bond lengths are closer, one may expect that $Fe^{3+}$ dopants in $LiAl_yCo_{1-y}O_2$ solid solutions will adopt nearly the same bond length, which is higher than that of Co−O and Al−O. This means that the main difference in the local environment of $Fe^{3+}$ dopants will be the extent of trigonal distortion of the $FeO_6$ octahedron. To rationalize the suggested local environment of $Fe^{3+}$ in $LiAl_yCo_{1-y}O_2$, Figure 7 gives the dependence of the $D$ parameter on the trigonal angle after fixing the Fe−O bond length to the Co−O, Al−O, $Al_{0.8}Co_{0.2}$−O, and Fe−O bond lengths in layered $LiCoO_2$, $LiAlO_2$, $LiAl_{0.8}Co_{0.2}O_2$, and $LiFeO_2$. For the sake of comparison, the same figure represents the experimentally extracted $D$ values for $Fe^{3+}$ in layered $LiAl_yCo_{1-y}O_2$ oxides. As one can see, at the fixed Fe−O bond length, the observed changes in $D$ values can be explained by the variation in the trigonal angle of no more than 4°. The higher extent of trigonal distortion of the $FeO_6$ octahedron is achieved for $Fe^{3+}$ dopants in Al-rich oxides, $LiAl_{0.8}Co_{0.2}O_2$. With the increase in the Co content, there is a discrete decrease in the trigonal distortion of the $FeO_6$ octahedron.

The discrete distortion of the $FeO_6$ octahedron can be associated with the effect of the first metal neighbors in the layer (Figure 6). In the metal layers, every $Fe^{3+}$ ion has six metal neighbors at a distance $a$ ($a$, unit cell parameter). Figure 8 shows the dependence of the $D$ parameter of $Fe^{3+}$ on the number of Al neigbors in the first metal shell. The relation between the ZFS parameter and the local environment of $Fe^{3+}$ (eq 3) indicates that the trigonal distortion of the $FeO_6$ octahedron increases gradually with the number of Al in the first metal sphere. Taking into account the two end $6Co^{3+}$ and $6Al^{3+}$ environments, there is a tendency for the suppression of rhombicity (expressed by $E/D$) of the $FeO_6$ octahedron, when Fe's are surrounded by Al neighbors (Table 1). The rhombicity of $FeO_6$ in mixed Co/Al environments displays a complex dependence, especially for oxides containing 50% Al. The origin of the rhombic distortion of the $FeO_6$ octahedron in a Co-rich environment is not clear. It is worth mentioning that, for $LiCo_{1-y}Fe_yO_2$ solid solutions, $Fe^{3+}$ ions with isomer shifts smaller than that of octahedrally coordinated $Fe^{3+}$ have been detected by Mössbauer spectroscopy.[8,12,14] Their appearance has been associated with $Fe^{3+}$ located in defect crystal sites: pseudotetrahedral position in $LiO_2$ layers or in square-pyramidal sites (in $CoO_2$ layers) formed with the participation of an oxygen vacancy.[12,14]

In addition, the local distortion of the $FeO_6$ octahedra is also sensitive toward the operating temperature: at lower temperature the $FeO_6$ octahedra are more distorted. The physical meaning of this issue is not clear, since there

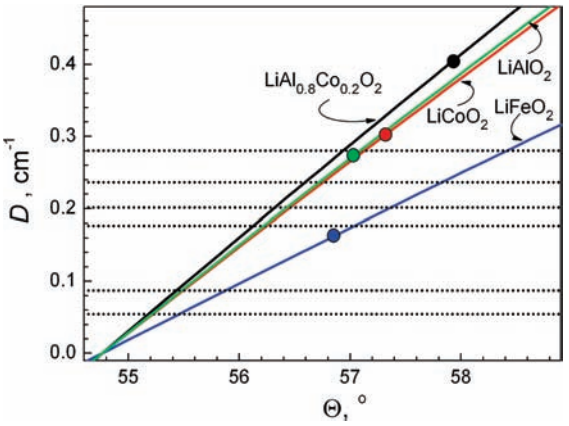


**Figure 7.** The dependence of the axial ZFS parameter ($D$) on the trigonal distortion angle by fixing the Fe−O bond length equal to that in $LiAl_{0.8}Co_{0.2}O_2$, $LiCoO_2$, $LiAlO_2$, and $LiFeO_2$. The full circles denote the calculated $D$ values, if supposing that $Fe^{3+}$ occupies the transition metal position of $LiAl_{0.8}Co_{0.2}O_2$, $LiCoO_2$, $LiAlO_2$, and $LiFeO_2$ oxides with preservation of the host bond length and the trigonal distortion angle. Dotted lines correspond to experimentally determined $D$ values.

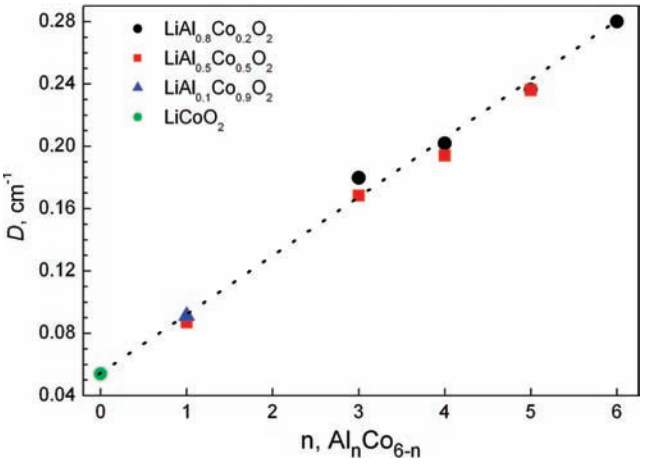


**Figure 8.** The $D$ values for $Fe^{3+}$ in $LiAl_yCo_{1-y}O_2$ versus the number of Al included in the first metal $[Co_{6-n}Al_n]$ environment.

are no data on the crystal structure of $LiAl_yCo_{1-y}O_2$ at lower temperature. However, the lack of any peculiarities in the magnetic susceptibility[43] and the electrical conductivity[44] of $LiCoO_2$ implies that no massive structural changes proceed at low temperatures. This means that local distortion takes place without affecting the long-range trigonal distortion of the layers.

The discrete changes in the trigonal distortion and rhombic component of the $FeO_6$ octahedron along the Al substitution bear resemblance with the discrete strengthening and distortion of the crystal field of $Ni^{3+}$ ions used as spin probes in the same matrix ($LiAl_yCo_{1-y}O_2$).[15] The local tetragonal distortion can be observed when $Ni^{3+}$ spin probes are located in a mixed $Co_{6-y}Al_y$ environment. The strength of the crystal field for $Ni^{3+}$ increases gradually, and the extent of the tetragonal distortion shows a tendency to increase with the progressive replacement of Co by Al. The observed different

(42) Douakha, N.; Holzapfel, M.; Chappel, E.; Chouteau, G.; Croguennec, L.; Ott, A.; Ouladdiaf, B. *J. Solid State Chem.* **2002**, *163*, 406–411.

(43) Levasseur, S.; Ménétrier, M.; Shao-Horn, Y.; Gautier, L.; Audemer, A.; Demazeau, G.; Largeteau, A.; Delmas, C. *Chem. Mater.* **2003**, *15* 348–354.

(44) Carewska, M.; Scaccia, S.; Croce, F.; Arumugam, S.; Wang, Y.; Greenbaum, S. *Solid State Ionics* **1997**, *93*, 227–237.

local distortions for $Fe^{3+}$ and $Ni^{3+}$ spin probes in layered $LiAl_yCo_{1-y}O_2$ are a consequence of their different electronic structures: $Fe^{3+}$ is an orbital singlet with a spin state higher than 1/2, while the low-spin $Ni^{3+}$ ion is an orbital doublet with $S = 1/2$. In the trigonal layers, the doubly degenerated ground state of $Ni^{3+}$ is unstable, a result of which being that a local tetragonal distortion is achieved. It is noticeable that a higher local distortion takes place when $Fe^{3+}$ and $Ni^{3+}$ spin probes are surrounded by $Al^{3+}$ ions only. On the other hand, these studies demonstrate the applicability of HF-EPR spectroscopy to local structural analysis of layered $LiAl_yCo_{1-y}O_2$ oxides.

## Conclusions

The multifrequency EPR studies of $Fe^{3+}$ spin probes in layered $LiAl_yCo_{1-y}O_2$ allow for distinguishing between several $Fe^{3+}$ ions in respect to axial and rhombic ZFS. Along the progressive replacement of Co by Al, the axial $D$ parameter increases, while the rhombic $E$ parameter shows a tendency to decrease. For all $LiAl_yCo_{1-y}O_2$ oxides, the $D$ parameter is positive, indicating that $Fe^{3+}$ occupies a trigonally compressed octahedron site in $Al_yCo_{1-y}O_2$ layers. The first metal coordination sphere becomes important, and the nature of the atoms in their positions causes the local trigonal and rhombic distortion around $Fe^{3+}$ ions. In a pure Co environment, $Fe^{3+}$ spin probes exhibit a lower extent of trigonal distortion, but a high rhombic component. The maximum trigonal distortion for the $FeO_6$ octahedron was achieved when $Fe^{3+}$ spin probes were surrounded by Al. On the same order, the rhombic component decreases.

**Acknowledgment.** The authors are indebted to the National Science Fund of Bulgaria (Contract no. Ch1701/2007) for financial support. The high-frequency EPR measurements carried out at the High Magnetic Field Laboratory in Grenoble, France, were supported by the European Commission within the sixth framework programme "Transnational Access − Specific Support Action" (contract No. RITA-CT-2003-505474) − "Access to research in very high magnetic field".